Materials Advances

ROYAL SOCIETY OF CHEMISTRY

COMMUNICATION

View Article Online
View Journal | View Issue

Cite this: *Mater. Adv.*, 2023, **4**, 476

Received 8th October 2022,
Accepted 10th December 2022

DOI: 10.1039/d2ma00959e

rsc.li/materials-advances

A new non-complex synthesis of NiO nanofoams for hydrogen storage applications†

Alisson S. Thill,[a] Dirléia S. Lima,[b] Oscar W. Perez-Lopez,[b] Robinson L. Manfro,[c] Mariana M. V. M. Souza,[c] Daniel L. Baptista,[a] Bráulio S. Archanjo,[d] Fernanda Poletto[e] and Fabiano Bernardi *[a]

The use of nanofoams is beneficial for a wide range of applications ranging from catalysis to plasmonics. The present communication reports on the non-complex synthesis of NiO nanofoams and their use for hydrogen storage applications. The results point to an improved hydrogen storage capacity at room temperature and ambient pressure of hydrogen as compared to Ni-based systems in the literature. DFT calculations point to a quasi-molecular bonding of the H_2 molecule at the surface of the NiO nanofoams. The results open new possibilities for the design of future smart materials for hydrogen storage applications and other fields.

Nanofoams are three-dimensional structures built by interconnected nanoparticles and/or nanometric filaments.[1] This specific class of nanomaterials draws attention due to their low density, high surface area, and high porosity, which enhances the surface activity and gas diffusion through the nanofoam.[1] These unique properties make them interesting materials for a wide range of applications like catalysis,[2] plasmonics,[3] sensors,[4] and energy storage.[5] In the literature, the synthesis methods existing are typically devoted to metal nanofoams, besides presenting complex procedures and/or using dangerous precursors with high environmental risks.[1,6] A few studies have been conducted on the synthesis of NiO nanofoams, which have already demonstrated their high capacity as glucose sensors,[7] as gas sensors,[4] and in lithium ion batteries.[5,8] The development of a non-complex synthesis method of NiO nanofoams may open new frontiers in catalysis, gas sensors, lithium ion batteries and energy storage applications.

Hydrogen has attracted an enormous scientific interest mainly due to the possibility of using it as a renewable and sustainable fuel to replace fossil fuels. It presents a very high energy storage capacity[9] and it can be produced in distinct ways, like through the photocatalytic water splitting reaction.[10] However, the main drawback that prevents hydrogen from being economically viable today is its storage.[9] The hydrogen storage system is a system able to store and release hydrogen under mild conditions ($-40\ ^{\circ}C < T < 60\ ^{\circ}C$ at 1 atm). For mobile applications, the conventional hydrogen storage methods (gaseous or liquid state) can only be economically viable for heavy vehicles, where the space occupied by the storage system does not represent a great issue. However, solid materials represent a promising alternative to the conventional methods.[11] In these materials, the hydrogen should be easily adsorbed and desorbed, which means the existence of a hydrogen binding energy at the surface of the material in the range of 0.2–0.6 eV.[12] Aiming to fulfill this requirement, scientists are searching for materials able to form quasi-molecular bonding with hydrogen instead of physisorption or chemical bonds, thus allowing their use under mild conditions.[12]

Carbon-based materials are very interesting candidates for hydrogen storage applications due to their high surface area, hydrogen storage capacity, low density, high thermal and chemical stability, and their ability to be manufactured in large quantities at low costs.[11] In particular, activated carbon draws a lot of attention due to its intrinsic interaction with H_2 molecules that is stronger than in other carbon-based materials.[13] However, activated carbon alone can only store hydrogen efficiently at very low temperatures or very high pressures.[14] Nanomaterials are supported on activated carbon aiming to improve its hydrogen storage properties at room temperature and ambient pressure, which occurs thanks to the hydrogen spillover effect.[15] Nevertheless, there is still a long and tedious way to go towards the synthesis of new materials with high hydrogen storage capacity under mild conditions. In view of the

[a] *Programa de Pós-Graduação em Física, Instituto de Física, Universidade Federal do Rio Grande do Sul, Brazil. E-mail: bernardi@if.ufrgs.br*
[b] *Departamento de Engenharia Química, Escola de Engenharia, Universidade Federal do Rio Grande do Sul, Brazil*
[c] *Departamento de Processos Inorgânicos, Escola de Química, Universidade Federal do Rio de Janeiro, Brazil*
[d] *Divisão de Metrologia de Materiais, Instituto Nacional de Metrologia, Qualidade e Tecnologia, Brazil*
[e] *Departamento de Química Orgânica, Instituto de Química, Universidade Federal do Rio Grande do Sul, Brazil*

† Electronic supplementary information (ESI) available: Experimental and theoretical procedures, data analysis and SAXS, TGA, hydrogen adsorption measurement, and TPD results. See DOI: https://doi.org/10.1039/d2ma00959e

above, a non-complex synthesis method of nanofoams may be very promising for hydrogen storage applications, especially due to the high permeability of the hydrogen molecules through the porous structure.

NiO nanofoams were synthesized by reducing the nickel(II) chloride hexahydrate salt ($NiCl_2{\cdot}6H_2O$) with glucose ($C_6H_{12}O_6$) and using the phytantriol/water system as a template (Fig. 1). Phytantriol is an amphiphilic molecule that shows a complex phase ternary diagram when water is added.[16,17] The phytantriol/water system presents liquid crystalline phases with supramolecular structures that can be selected by the water amount and temperature used. The inverse bicontinuous cubic phase with space group $Ia\bar{3}d$ (Q^G_{II}) of the phytantriol/water system was chosen as a template due to the presence of nanometric size channels,[17,18] where the nucleation process is expected to take place, then representing a promising system for the formation of nanofoams. A solution with 75 mg of $NiCl_2{\cdot}6H_2O$ and a solution with 120 mg of $C_6H_{12}O_6$, both in 3 mL of water ("type 1" ultrapure grade), were prepared. The $NiCl_2{\cdot}6H_2O$ solution was added to a mixture of 54 g of phytantriol + 7 mL of water ("type 1" ultrapure grade) and mixed using a spatula. Then the $C_6H_{12}O_6$ solution was added to the $NiCl_2{\cdot}6H_2O$ + phytantriol solution aiming to obtain the Q^G_{II} phase[17] of phytantriol with 20 wt% of water. The Small Angle X-ray Scattering (SAXS) pattern of the sample immediately after phytantriol and glucose addition shows the presence of the inverse bicontinuous cubic phase with space group $Ia\bar{3}d$ (Q^G_{II}), as expected (Fig. S1 of the ESI†). The system was left to react during 20 hours at 25 °C. Then, in order to remove the phytantriol phase and to obtain the NiO nanofoams, the system was calcined at 500 °C for 4 hours in a muffle furnace. The temperature was determined from Thermogravimetric analysis (TGA) measurements (see Fig. S2 of ESI†). This procedure allows the non-complex synthesis of nanofoams, without dangerous or environmentally risky reagents, and it is extendable to different systems. It is important to stress that the liquid crystalline phase can be easily selected through the water amount and temperature used during synthesis, thus enabling nanofoams with distinct properties.

Scanning Transmission Electron Microscopy (STEM) and Transmission Electron Microscopy (TEM) images were acquired aiming to probe the structure formed in the synthesis. Fig. 2(a) shows a typical STEM image where it is possible to observe inhomogeneous nanostructures built by bright and dark regions. Zooming in on the region with the STEM (Fig. 2(c)) and TEM (Fig. 2(b)) techniques allows observation that the nanostructures are formed by interconnected nanoparticles of elongated shape, as observed in nanofoams. The nanofoams present a typical length of around 50 nm and channel diameters of around 10 nm. The comparison between a single nanostructure (Fig. 2(c)) with the representation of the inverse bicontinuous cubic phase of phytantriol (Fig. 2(d)) shows high similarity between both structures, thus strengthening that the

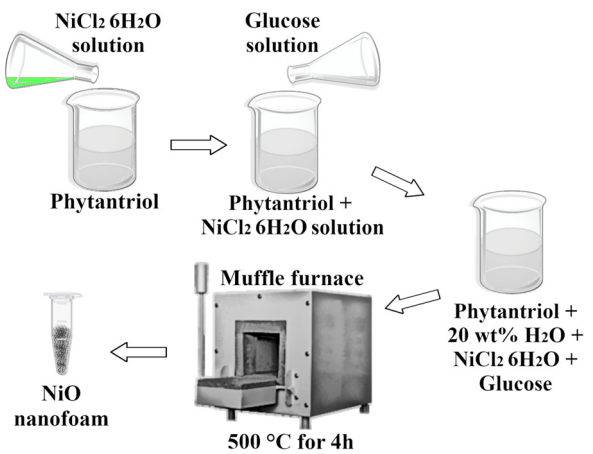

Fig. 1 Schematic representation of the synthesis procedure of the NiO nanofoams.

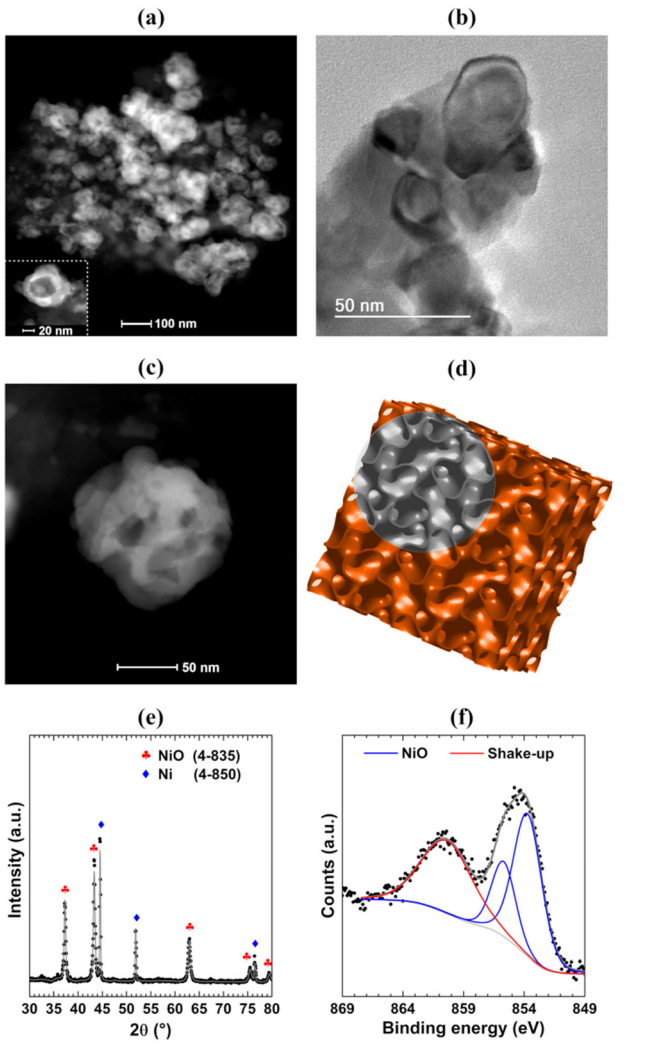

Fig. 2 Typical (a) STEM and (b) TEM image of the NiO nanofoams synthesized with a single nanostructure highlighted in the inset of part (a). Comparison between (c) the STEM image of a single nanostructure and (d) the schematic representation of the inverse bicontinuous cubic phase of phytantriol. (e) XRD pattern and (f) XPS spectrum at the Ni $2p_{3/2}$ region of the NiO nanofoam synthesized.

phytantriol phase acts as a template for the synthesis of NiO nanofoams. Fig. 2(e) presents the X-Ray Diffraction (XRD) pattern indexing and the corresponding Rietveld refinement. The NiO cubic phase is the main phase (73%) existing in the nanofoams synthesized, which shows also the presence of the Ni metallic phase contributing 27%. The mean crystallite size of NiO obtained from Rietveld refinement is 48 nm, which is in accordance with the size of the nanofoam structures observed in the STEM images (Fig. 2(b) and (c)). Fig. 2(f) shows the Ni $2p_{3/2}$ XPS spectrum of the NiO nanofoams with the presence of a single NiO component located around 854.0 eV,[19] which comes due to the surface sensitivity of the XPS technique (λ = 1 nm for photoelectrons coming from the Ni $2p_{3/2}$ electronic level). This means that the nanofoams are composed of a metallic Ni core and a NiO shell since there is no metallic component observed at the Ni $2p_{3/2}$ XPS region. Consequently, NiO is the single phase participating in the hydrogen storage process and hereafter the sample will be labeled as NiO nanofoam. These results demonstrate that the synthesis method was successfully employed for synthesizing NiO nanofoams and may be even expanded to other metal or metal oxide systems with a variety of properties chosen from the phytantriol phase used.

The characteristics presented by the NiO nanofoams synthesized make this a promising system for hydrogen storage applications. The hydrogen adsorption experiment was conducted with 0.40 wt% NiO nanofoams supported on activated carbon charcoal, as determined by the Flame Atomic Absorption Spectrometry (FAAS) technique. A sample of pure activated carbon was also measured for comparison purposes. The NiO nanofoams present a gravimetric density of 7.0×10^{-2} wt% under mild conditions of room temperature and ambient pressure (Fig. S3 of the ESI†). This value represents an improvement of almost 4.4 times in comparison to the pure activated carbon case (1.6×10^{-2} wt%). Temperature-programmed desorption of hydrogen (TPD-H_2) measurements was also conducted and shows a gravimetric density of 7.8×10^{-2} wt%, in agreement with the previous results (Fig. S4 of the ESI†).

In the literature,[20–22] Ni-based systems can reach a gravimetric density of up to 3 wt% but only using temperatures (77 K) and pressures (up to 200 bar) very far away from those required for applications. It is hard to compare the gravimetric density results with those found in the literature for similar systems due to the different amounts of Ni, hydrogen pressures and temperatures used in each case. Nevertheless, it is possible to do a comparison with the value of the gravimetric density relative to the pure activated carbon case. The result of the present work (4.4) is clearly better than those presented in the literature for Ni-based/C systems. Zubizarreta *et al.*[20] studied hydrogen storage in activated carbon xerogels with selected characteristics and doped with different amounts of Ni. The hydrogen adsorption measurements were performed at 77 K with hydrogen pressure up to 40 bar, and at room temperature with hydrogen pressures from 10 bar to 200 bar. The comparison between pure activated carbon xerogels and activated carbon xerogels with Ni shows an improvement of only 1.3 times for the best case (77 K and 40 bar). Zielinsk *et al.*[21] studied the hydrogen storage properties of a commercial activated carbon impregnated with different amounts of Ni nanoparticles (1 wt%, 5 wt% and 10 wt%). The hydrogen adsorption measurements were performed at room temperature and at two different hydrogen pressures, 20 bar and 30 bar. The greatest amount of adsorbed hydrogen is around 3 times bigger than the pure activated carbon case. Rossetti *et al.*[22] studied the hydrogen storage in different metal nanoparticles (Cu, Ni, Pt, Pd and Rh) supported on activated carbon with different amounts (0.5 wt% and 2 wt%). The hydrogen adsorption measurements were performed at 77 K with two different pressures (4.9 bar and 19.6 bar) and at 273 K with four different pressures (5.9 bar, 20.6 bar, 40.2 bar and 98.8 bar). For Ni nanoparticles at 273 K, it was observed that the case presenting the greatest amount of adsorbed hydrogen was 0.5 wt% Ni nanoparticles, which presents around 3.3 times the amount of adsorbed hydrogen than that obtained for pure activated carbon at 98.8 bar. The present findings represent a great improvement in the hydrogen storage capacity, not only for the better results found in comparison to the activated carbon sample but also for obtaining the result for room temperature and ambient pressure of hydrogen. In addition, it is well known that the higher the hydrogen pressure, the higher the amount of adsorbed hydrogen in comparison to the pure activated carbon case and the current results may be further improved by decreasing the temperature.[20–22] This means that the NiO nanofoams represent a highly promising system for hydrogen storage applications.

Interestingly, the metallic Ni phase is typically used for hydrogen storage applications in the literature[20–22] instead of the NiO phase, but the current promising results were obtained with NiO nanofoams. Spin-polarized DFT calculations were performed using the Quantum-ESPRESSO 5.4.0 package[23] aiming to determine the H_2 adsorption energy at the surface of Ni and NiO atomic clusters and Ni(111) and NiO(100) slabs following the procedure described by Ramos-Castillo *et al.*[24] The Ni(111) and NiO(100) surface orientations were chosen because they represent the most stable ones for the Ni and NiO systems, respectively.[25,26] Fig. 3(a) and (b) present the H_2 adsorption energy for the Ni and NiO case, respectively, as a function of the H_2 adsorption site. The results for the Ni metallic case point to the chemisorption regime in the case of a Ni cluster or Ni(111) slab with bridge, hcp and hollow adsorption sites of the H_2 molecule. On the other hand, the desired quasi-molecular bonding regime can only be reached for the top adsorption site of the Ni(111) slab. This means that the replacement of Pd, widely used as a hydrogen storage material, by a cheaper metal like Ni is hard to accomplish in practice because there is a specific adsorption site for the quasi-molecular regime and the other adsorption sites, in the chemisorption regime, are more energetically favorable. Consequently, the quasi-molecular bonding of H_2 is barely achieved for metallic Ni. Fig. 3(b) shows that the NiO system also presents the chemisorption regime for a NiO cluster but the physisorption regime occurs for any adsorption site

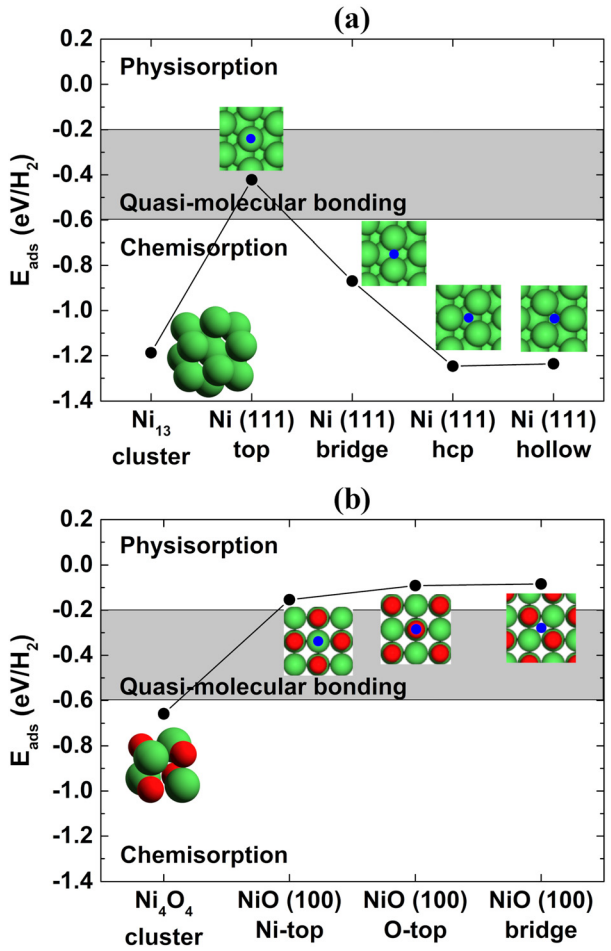

Fig. 3 H_2 adsorption energy as a function of the adsorption site of (a) Ni and (b) NiO systems. The blue circle represents the adsorption site of the H_2 molecule and the green and red circles represent the Ni and O atoms, respectively. The gray region represents the adsorption energy values corresponding to the quasi-molecular bonding of H_2 to the surface of the materials.

(Ni top, O top and bridge) of the NiO(100) slab. The NiO nanofoams synthesized in the present work are formed by interconnected nanostructures, as shown by the STEM and TEM images (Fig. 2(a)–(c)), and have only the NiO chemical component at the surface, as observed in the Ni $2p_{3/2}$ XPS region (Fig. 2(f)). The nanofoams can be modeled realizing that their smooth surface regions can possibly be described as NiO slabs, but the atomic edges with low coordinated sites (like a NiO cluster) of the interconnected nanostructures cannot be neglected, otherwise the system modeled would correspond to a thin film. This means that the nanofoams synthesized probably present a typical H_2 adsorption energy between these two extreme cases (NiO cluster and slab), rather than belonging to the desired quasi-molecular regime. The mechanism of hydrogen storage can be described with the initial H_2 adsorption at the NiO nanofoam surface. The H–H bonding increases from 0.75 Å to around 0.80 Å (depending on the adsorption site), as determined by DFT calculations. Besides the increase of the H_2 bond length, the molecule is not dissociated but it is stored as H_2 instead of H + H. The results show that both the NiO chemical state and nanofoam characteristics make the NiO nanofoams a very promising system for hydrogen storage applications. Furthermore, the NiO nanofoams can be easily synthesized, thus representing a strong candidate for supplying the current hydrogen storage needs.

This communication demonstrates a very simple method for synthesizing NiO nanofoams using the phytantriol/water system. The NiO nanofoams present promising results for hydrogen storage applications considering both the mild conditions used (room temperature and ambient pressure) and the comparison with literature results. This is explained due to the presence of both low coordinated sites and smooth surface regions of the NiO nanofoams, which indicates the existence of the quasi-molecular bonding regime for the hydrogen adsorption process. The quasi-molecular bonding of hydrogen with solid materials is the key factor for reaching the ultimate goal for hydrogen storage applications, and thus NiO nanofoam is a great material for boosting this field.

Author contributions

This manuscript was written through contributions of all authors. All authors have given approval to the final version of the manuscript.

Conflicts of interest

There are no conflicts to declare.

Acknowledgements

The authors acknowledge the use of the infrastructure of the CNANO-UFRGS, CM-UFMG, LAMAS-UFRGS, LAMAT-UFRGS, Central Analítica-IQ-UFRGS, NULAM/DIMAT-INMETRO and CESUP-UFRGS. A. S. T., and F. B. thank the CNPq for the research grant. The authors also thank CAPES – Finance Code 001.

References

1 B. C. Tappan, S. A. Steiner III and E. P. Luther, *Angew. Chem., Int. Ed.*, 2010, **49**, 4544.
2 A. Dutta, C. E. Morstein, M. Rahaman, A. Cedeño López and P. Broekmann, *ACS Catal.*, 2018, **8**, 8357.
3 J. Biener, G. W. Nyce, A. M. Hodge, M. M. Biener, A. V. Hamza and S. A. Maier, *Adv. Mater.*, 2008, **20**, 1211–1217.
4 X. Li, J. Tan, Y. Hu and X. Huang, *Mater. Res. Express*, 2017, **4**, 045015.
5 X. Guo, G. Zhang, Q. Li, H. Xue and H. Pang, *Energy Storage Mater.*, 2018, **15**, 171.
6 H. J. Koster, H. J. O'Toole, K. L. Chiu, T. Rojalin and R. P. Carney, *Colloid Interface Sci. Commun.*, 2022, **47**, 100596.
7 C. Guo, Y. Wang, Y. Zhao and C. Xu, *Anal. Methods*, 2013, **5**, 1644.

8 W. Ni, H. B. Wu, B. Wang, R. Xu and X. W. Lou, *Small*, 2012, **8**, 3432.
9 J. O. Abe, A. P. I. Popoola, E. Ajenifuja and O. M. Popoola, *Int. J. Hydrogen Energy*, 2019, **44**, 15072.
10 A. S. Thill, W. T. Figueiredo, F. O. Lobato, M. O. Vaz, W. P. Fernandes, V. E. Carvalho, E. A. Soares, F. Poletto, S. R. Teixeira and F. Bernardi, *J. Mater. Chem. A*, 2020, **8**, 24752.
11 Y. Kojima, *Int. J. Hydrogen Energy*, 2019, **44**, 18179.
12 P. Jena, *J. Phys. Chem. Lett.*, 2011, **2**, 206.
13 M. Mohan, V. K. Sharma, E. A. Kumar and V. Gayathri, *Energy Storage*, 2019, **1**, e35.
14 H. G. Schimmel, G. J. Kearley, M. G. Nijkamp, C. T. Visser, K. P. de Jong and F. M. Mulder, *Chem. – Eur. J.*, 2003, **9**, 4764.
15 J. Ren, N. M. Musyoka, H. W. Langmi, M. Mathe and S. Liao, *Int. J. Hydrogen Energy*, 2017, **42**, 289.
16 S. Akbar, A. Anwar, A. Ayish, J. M. Elliott and A. M. Squires, *Eur. J. Pharm. Sci.*, 2017, **101**, 31.
17 J. Barauskas and T. Landh, *Langmuir*, 2003, **19**, 9562.
18 B. J. Boyd, D. V. Whittaker, S. M. Khoo and G. Davey, *Int. J. Pharm.*, 2006, **309**, 218.
19 A. N. Mansour, *Surf. Sci. Spectra*, 1994, **3**, 231.
20 L. Zubizarreta, J. A. Menéndez, N. Job, J. P. Marco-Lozar, J. P. Pirard and J. J. Pis, *Carbon*, 2010, **48**, 2722.
21 M. Zieliński, R. Wojcieszak, S. Monteverdi, M. Mercy and M. M. Bettahar, *Int. J. Hydrogen Energy*, 2007, **32**, 1024.
22 I. Rossetti, G. Ramis, A. Gallo and A. Di Michele, *Int. J. Hydrogen Energy*, 2015, **40**, 7609.
23 P. Giannozzi, S. Baroni, N. Bonini, M. Calandra, R. Car, C. Cavazzoni, D. Ceresoli, G. L. Chiarotti, M. Cococcioni and I. Dabo, *J. Phys.: Condens. Matter*, 2009, **21**, 395502.
24 C. M. Ramos-Castillo, J. U. Reveles, R. R. Zope and R. De Coss, *J. Phys. Chem. C*, 2015, **119**, 8402.
25 Y. N. Wen and J. M. Zhang, *Solid State Commun.*, 2007, **144**, 163.
26 J. Xiang, B. Xiang and X. Cui, *New J. Chem.*, 2018, **42**, 10791.